Environmental Science and Pollution Research (2023) 30:79091–79105
https://doi.org/10.1007/s11356-023-27691-x

RESEARCH ARTICLE

Removing of cationic dyes using self-cleaning membranes-based PVC/nano-cellulose combined with titanium aluminate

Aya Abd El Aziz Elfiky[1] · Mahmoud F. Mubarak[1] · Mohamed Keshawy[1] · Ibrahim El Tantawy El Sayed[2] · Thanaa Abdel Moghny[1]

Received: 22 November 2022 / Accepted: 12 May 2023 / Published online: 7 June 2023

Abstract

This research used the phase inversion approach to construct polyvinyl chloride nanocellulose@titanium aluminate nanocomposite membranes (PVC/NC@TALCM) to adsorb and filter dye from wastewater. FTIR, XRD, and SEM were used to determine the adsorptive nanocomposite membrane that had been synthesized. The thermal and electrical properties measurements were carried out using a static system. The influence of several adsorbent dosages, pH, and dye concentrations on the nanocomposite membrane's adsorption ability was investigated. Using a dead-end filtration system, the PVC-NC@TALCM was evaluated as a pressure filtration membrane system. It was found that 98.6% of MB dye was removed by PVC-NC@TALCM membrane, which was loaded with 5% titanium aluminate at pH 10. The kinetic adsorption studies indicated that the adsorption of MB onto the PVC-NC@TALCM nanocomposite membrane obeys pseudo-second-order that indicates the chemosorption process. The isotherm data were described using Freundlich and Langmuir models, and the Freundlich isotherms were shown to be more closely match the experimental data than the Langmuir model. Finally, the PVC-NC@TALCM nanocomposite membrane was economical, environmentally friendly, and self-cleaning.

Keywords Self-cleaning · Nanocomposite · Membrane · Nanofiltration · Hydrophobicity · Cationic dye

Abbreviations

PVC-NC@TALCM	Polyvinyl chloride nanocellulose@titanium aluminate
PVC	Polyvinyl chloride
NC	Nanocellulose
Ti_2ALO_4	Titanium aluminate
THF	Tetrahydrofuran
DMF	Dimethylformamide

Introduction

Wastewater is a major concern as it contains pollutants that harm the environment and human health around the world. High amounts of dyes, heavy metals that discharged into water bodies, create substantial health and environmental problems, as well as a rise in wastewater treatment costs. Thereby, the removing of dyes and heavy metals from drinking and wastewater is essential for environmental and human health protection (Sunil et al. 2021).

Researchers have used standard techniques for treating dye solutions, such as ultrafiltration membrane, ion exchange, electrocoagulation, advanced oxidation, photocatalytic degradation, coagulation and flocculation, and phytoremediation (Teng et al. 2022). However, the abovementioned methods are unsuccessful due to the processing of large quantities of sludge, harmful by-products, bio-resistant organisms, and complex operational procedures (Oladoye et al. 2022). Due to its low cost, membrane nanofiltration has long been a promising technique in industrial wastewater treatment areas (Gidstedt et al. 2022).

The membrane filtration method suffers from concentration polarization and membrane fouling, leading to a

Responsible Editor: Angeles Blanco

✉ Aya Abd El Aziz Elfiky
aya.elfiky91@yahoo.com

[1] Petrolum Applications Department, Egyptian Petroleum Research Institute (EPRI), Ahmed El-Zomer, Nasr City, Cairo, Egypt

[2] Department of Chemistry, Faculty of Science, Menoufia University, 32511, Shebin El Koom, Menoufia, Egypt

decrease in separation efficiency, an increase in operating costs, and a shortening of membrane lifetime. Polymeric membranes are extensively employed in water purification and wastewater treatment (Pan et al. 2022).

Membrane types such as microfiltration, nanofiltration, ultrafiltration, catalytic, and conducting membranes have been developed for wastewater treatment and bio-processing (Wang et al. 2021). This paper created a one-step impregnation of nanomaterials such as nanocellulose on membrane surfaces to provide self-cleaning properties when exposed to polluted wastewater (Wang et al. 2022a, b, c).

Polyvinyl chloride membranes (PVC) are widely used due to their hardness, resistance to abrasion, acid, alkali, and microbial corrosion, but their hydrophobicity can cause fouling when processed with protein-like substances (Pankiew et al. 2021). In addition, PVC has gained research attention as a separation membrane due to its low biofouling propensity. Self-cleaning membranes provide a solution to the challenge of keeping membranes permeable, clean, and functional (Nthunya et al. 2022).

Cellulose is the most prevalent polymeric raw material derived from the biosphere. It is composed of crystalline cellulose, hemicellulose, lignin, mineral, wax, and ash. Nanocellulose (NC) can be used as an adsorbent material for water treatment, attaching pollutants such as heavy metal ions and dyes (Perumal et al. 2022).

The composite technique of impregnating porous substrates with multiple NC grades has sparked renewed interest in producing adsorbents (Chen et al. 2022). Nanometal oxides such as TiO_2 nanoparticles are potent inorganic materials, boosting permeability, surface hydrophilicity, mineralization, and self-cleaning/antifouling capabilities (Voisin et al. 2021).

This research aims to prepare a new nanocomposite membrane filter based on PVC/nano cellulose and titanium aluminate. Such membrane will be evaluated as an adsorbent to remove MB dye at different concentrations. The Effect of the $TiAl_2O_4$ concentration on the physical and chemical properties of the membranes will be studied. Parameters such as dye concentration, pH, membrane dose, and temperature will be studied. Various isothermal and kinetic models will be applied to verify the adsorption behavior and desorption process. Experimental results of dye batch adsorption will be investigated using PVC-NC @ TALCM membrane.

Experimental

Materials

The agricultural wastes were received from Egyptian farms as the source of cellulose. Polyvinyl chloride (PVC), tetrahydrofuran (THF), dimethyl formamide (DMF), sodium hydroxide (NaOH), titanium acetate $Ti(CH_3COO)_2.2H_2O$, ammonium hydroxide NH_4OH, titanium chloride ($TiCl_4$), and methylene blue (MB) from Sigma Aldrich were utilized throughout the investigation. Distilled water from the central lab was also employed. Other chemical products were used, such as distilled water, HCl, isopropyl alcohol, and NH_4OH (25%) solutions. In this work, all of the chemicals were used under analytical grade.

Purification of agricultural wastes

Agricultural wastes with varying cellulose concentrations, such as rice straw, were collected and dried in the sun before being chopped into little pieces (1–3 mm) (Debnath et al. 2021). The cut wastes were washed with distilled water and acetone, then dried overnight in an oven at 60 °C and chosen for other cellulose. Ten grams of the cellulosic materials undergo to alkali treatment with 250 ml sodium hydroxide (1% wt/v) solution for 5 h and refluxed at 120 °C to remove the hemicelluloses. The insoluble residue (cellulose) was collected by filtering at the end of the extraction and rinsed extensively with distilled water until the filtrate was neutral. The resultant cellulosic materials were dried in the air before being mixed with dimethylsulfoxide (DMSO) and heated in a water bath at 80 °C for 3 h. The product was then filtered, washed with distilled water, and air-dried (Shaheen and Emam 2018).

Preparation of nanocellulose

Nanocellulose (NC) was synthesized in spherical form rod-like highly crystalline nanocrystals. In this respect, 5 g of nanocellulose was obtained from 15 g of lignocellulosic material by acid hydrolysis and refluxing of dignified and hemicellulose (free cellulose) with 250 ml of 5 N sulfuric acid for 5 h at 50 °C under vigorous agitation to remove amorphous area and form cellulose nanocrystals as shown in Fig. 1. The hydrolysis was stopped by adding fivefold the quantity of water to the reaction mixture. Before centrifugation, the resulting mixture was allowed to cool to room temperature. The fractions were cleaned with distilled water and centrifuged regularly. After at least five washing cycles, centrifugation ended, and the supernatant liquor became turbid (Vincent and Kandasubramanian 2021).

Preparation of titanium dioxide nanoparticles via sol–gel method

Briefly, to prepare a titanium acetate solution, 20 g Ti $(CH_3COO)_2\ 2H_2O$ was combined with 150 ml distilled water and agitated for 20 min at 35 °C. To prepare the NaOH solution, 80 g (1% w/v) NaOH powders were dissolved in 80 ml water and stirred for 20 min at 35 °C. Both resolutions were

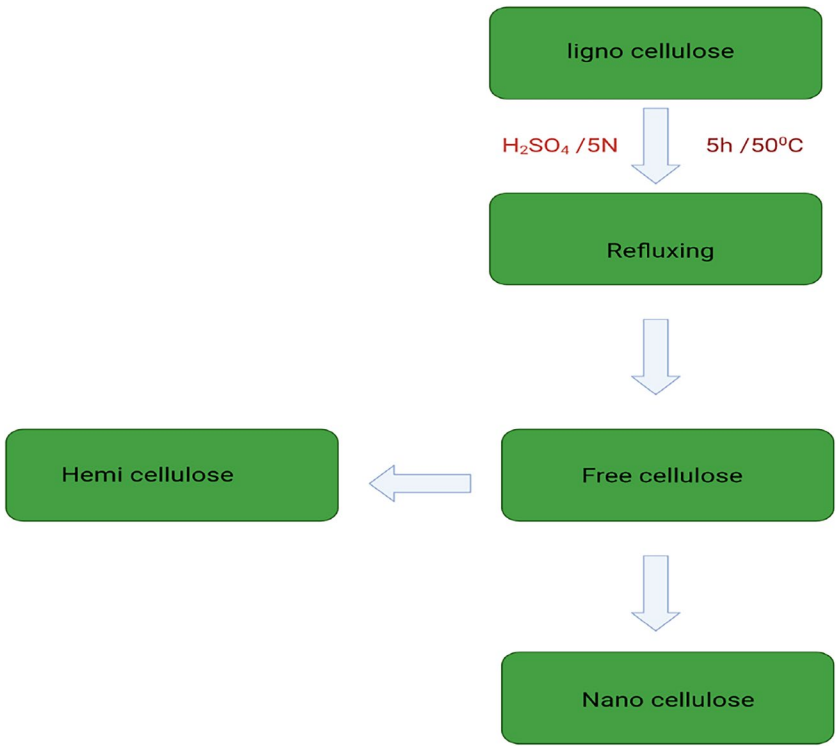

Fig. 1 Preparation of nanocellulose

mixed gently, and the titration reaction went smoothly, with 100 ml ethanol added drop-by-drop and vigorous stirring for 90 min until a gel-like result was obtained. To create TiO_2 nanoparticles, the gel was dried at 80 °C overnight and calcinated at 250 °C in the furnace for 4 h (Tesfaye Jule et al. 2021). Figure 2 depicts the production of TiO_2 nanoparticles using NaOH and is expressed by the following Eq. 1.

$$Ti(CH_3COO)_2.2H_2O + 2NaOH \rightarrow TiO_2 + 2NaCH_3COO + H_2O \quad (1)$$

Synthesis of titanium aluminate nanocomposite

Although metallic alkoxides have high reactivity with water, which favors the hydrolysis process and results in the immediate precipitation of the metallic hydroxide, the alkoxides were employed as precursors in the synthesis of titanium aluminate in our work. In this regard, 43.92 g of titanium sec-butoxide and 63.57 g of aluminum sec-butoxide were transferred to a 1-L three-necked glass flask. After that, in the glove box, these alkoxides were shaken well under a

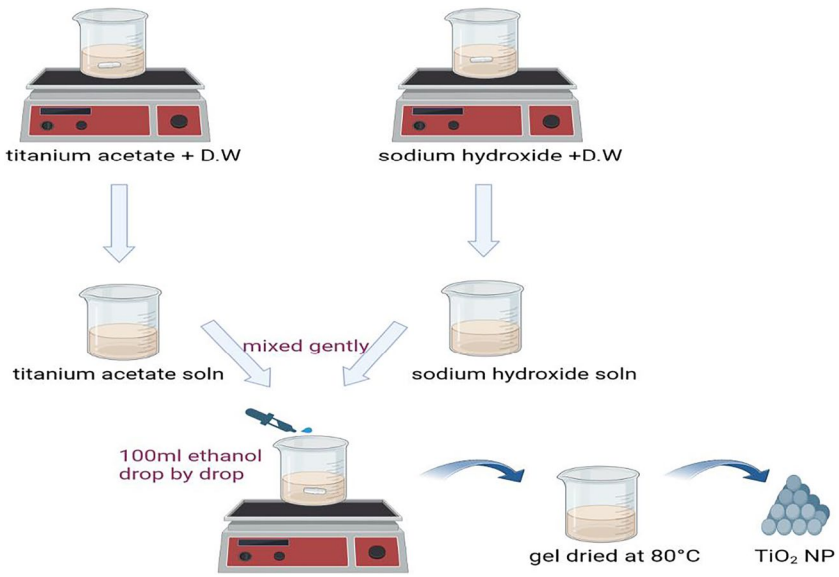

Fig. 2 Titanium dioxide nanoparticle preparation

nitrogenous atmosphere in the three-ended balloon with a Teflon blade coated with thin-film metallic glass (TFMG) for 30 min to be homogenized. The alkoxides moisture will become almost viscous and exhibit yellow transparent color. To solve the alkoxides moisture, add 100 ml isopropyl alcohol and shake for another 2 h. Finally, 30 ml of 1.7 M H_2O and 0.5 M HCI and solution in isopropyl alcohol solution were added under constant shaking to avoid the inactivity atmosphere of the balloon (Ha et al. 2020).

Composite membranes fabrication

The asymmetric membranes were made using the phase inversion approach as the following: the polymer solution, which included polyvinyl chloride (PVC) and nanocellulose (NC), was dissolved in dimethyl formamide (DMF), and the mixture was then mixed with titanium oxide nanoparticles and rapidly agitated for 24 h at 60 °C, as shown in Table 1, before being manually cast with a 150-mm-thick casting knife at room temperature on a clean glass plate. As illustrated in Fig. 3, for free-convective solvent evaporation, the membrane surface was exposed to air at ambient temperature (about 26 °C. After 60 s delay, a distilled water bath submerged the membranes at 26 °C. After 15 min, the polymeric skin layer was removed and immersed in distilled water for 24 h to remove all residual solvents (Deng and Li 2021). Digital caliper equipment (Electronic outside Micrometer, IP54 type OLR) was used to measure the thickness of the final membrane between 135 and 150 mm. Two processes must be completed to obtain the final membrane: first, the contact angle concentration must be optimized to get a membrane with the highest rejection and flux. The second stage examines the influence of different nanoparticle adsorbent concentrations on dye rejection (Sun et al. 2021).

Membrane characterization

FTIR spectral analysis of membrane was performed using FTIR, model (Thermo Scientific Nicolet iS10 Spectrometer) produced by Thermo Fisher Scientific (USA) company in the spectral range from 4000 to 400 cm^{-1}, the beam splitter is KBr/Ge mid-infrared optimized, with resolution 4 cm^{-1} (Park et al. 2021). X-ray diffraction (XRD) was employed to obtain the phases of the samples. X-ray diffraction (Philips PW3040/60 X, pert PRO P Analytical-Netherlands) was used to obtain the patterns. Continuous measurements were taken from 5 to 90° while the samples were on a glass slide. (Jain et al. 2022). All samples were observed by scanning electron microscope (SEM) model (Zeiss evo 10) attached with energy dispersive X-ray analysis (EDX) unit, with accelerating voltage 500 kV magnification14 × up to 100,000 × (Agarwalla and Mohanty 2022). TGA analysis

Table 1 The composition of the membrane casting solution

Membrane sample no	PVC (%w/w)	NC (%w/w)	$TiAl_2O_4$(%w/w)	(wt%) DMF
1	15	0	0	100
2	15	0.15	0	100
3	15	0.15	0.15	100
4	15	0.15	0.45	100
5	15	0.15	0.75	100

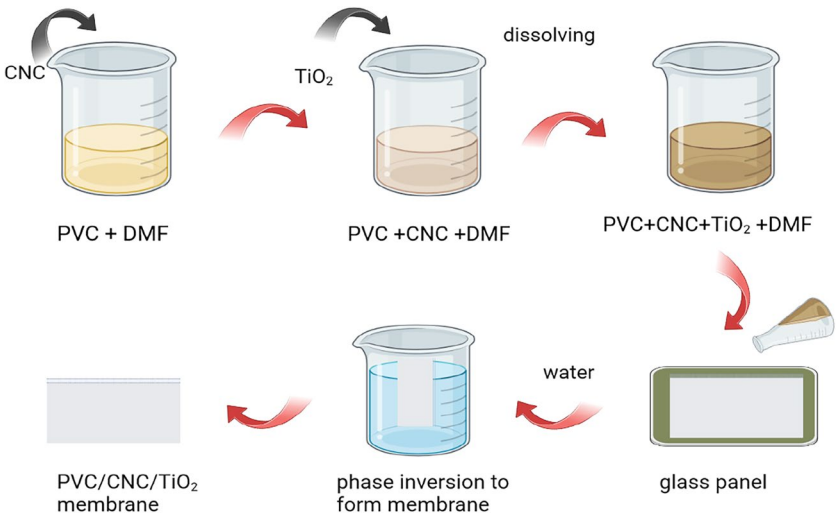

Fig. 3 Preparation of nanocomposite membrane

was performed on the Perkin-Elmer TGA7 thermo balance. The dried samples were analyzed under a nitrogen atmosphere in the temperature range of 5–600 °C at a scanning rate of 20 °C/min.

Dye adsorption experiments

At room temperature, 0.1 g of a PVC-NC@TALCM membrane was submerged in 50 mL of MB solution and swirled at 400 rpm. The free MB was analyzed at a wavelength of 664 nm and at different time intervals using UV–a visible spectrophotometer Shimadzu (UV-2600).

The influence of changing the initial dye concentrations (10, 15, 20, 25, 30 ppm), adsorbent dose (0.1, 0.5, 0.8 g), and pH (5, 7, 9) were studied. From Eqs. 2 and 3, both dye uptake efficiency ($R\%$) and the adsorption capacity (q_e) can be calculated.

$$q_e = \frac{(c_\circ - c_e)v}{w} \tag{2}$$

$$R(\%) = \frac{(c_\circ - c_e)}{c_\circ} \times 100 \tag{3}$$

where W is the membrane's weight (g), V is the volume (L), and the equilibrium and starting concentrations of MB dye are C_e (mg/L) and C_o, respectively [23].

Self-cleaning assessment property of PVC/NC@TiAl2O4 membrane through the contact angle measurement

Cut the PVC/NC@$TiAl_2O_4$ membrane to the desired size and clean it thoroughly. Measure the contact angle using a contact angle goniometer and software. Repeat the measurement several times to ensure consistency. Calculate the mean and standard deviation of the contact angle measurements and compare them to a control sample to determine if the membrane exhibits a self-cleaning property. A surface with a low contact angle (less than 90°) indicates that the surface is hydrophilic and likely to exhibit self-cleaning behavior (Ismail et al. 2022).

Result and discussion

FTIR analysis of nanocomposite membranes

The FTIR spectrum of PVC-NC and PVC-NC@TALCM membranes at different titanium aluminate concentrations is given in Fig. 4. Such spectrum exhibited bands at 2239 and 1331 cm^{-1}, that may be assign to CH_2's asymmetric stretching and deformation vibrations, respectively, and the absorption peaks appeared at 1031 and 829 cm^{-1}, may cause by CH's in-plane and out-plane bending modes, are the distinctive PVC's peaks. Whereas, the stretching vibration peak appeared at 3409 cm^{-1} may be the (OH) group of the nanocellulose. The two absorption peaks at around 1688 and 1401 cm^{-1} may be ascribed to the absorption of the bending vibrations of (C-O), as can be observed from the spectrum of PVC /NC) (Rana et al. 2021).

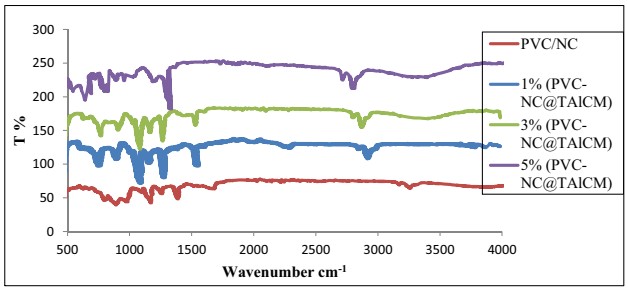

Fig. 4 FTIR of PVC/NC and PVC-NC@TALCM with different ratios (1, 3, 5%)

It is found that upon combining PVC/NC with $TiAL_2O_4$, the intensity of expansion – OH band increases from lower wavelengths 485, 486.4, and 479 cm^{-1}, and moves to a higher wavelength 683, 633.8, and 544.99 cm^{-1}, with increasing $TiAL_2O_4$ ratio from 1, 3, 5%, respectively. This may be due to the formation of hydrogen bonds between the hydroxyl groups of titanium aluminate with the aldehyde group of nanocellulose (Ahmad and Guria 2022).

XRD analysis of nanocomposite membranes

XRD pattern of PVC/NC in Fig. 5 shows a diffraction peak at 2θ of 17.3°, while the role of X-ray diffraction of the inorganic nanocomposite, e.g., $TiAl_2O_4$, can be investigated through the entire measurement range. In this regard, the

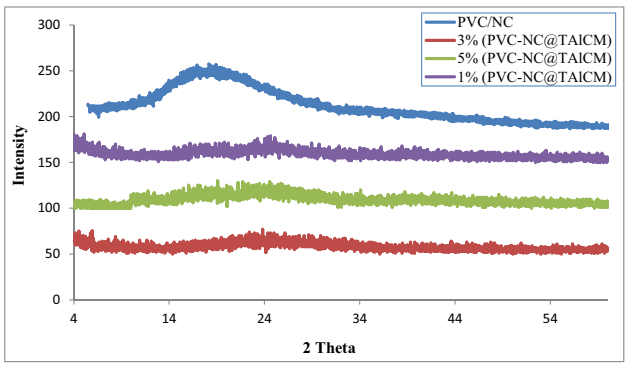

Fig. 5 X-ray diffraction scans of PVC/NC and PVC/NC filled with different concentrations of titanium aluminate

XRD diffraction patterns of PVC-NC@TALCM at 1%, 3%, and 5% of titanium aluminate exhibit the varied type of crystalline phase's peak; this reveals the presence of some crystalline peak indicating the complete homogenous distribution of $TiAl_2O_4$ in the PVC/NC membrane matrix. Furthermore, the increase in $TiAl_2O_4$% leads to a sharp, intense peak at about 2θ of 24.13, 25.93, and 33.5 for 1%, 3%, and 5% of $TiAl_2O_4$ respectively (Fahoul et al. 2021). Multiple peaks with lower intensities appear at 2Θ of 27.8, 34.6, 43.59, and 50.35, 38.17, and 48.55, attributed to (220) and (311) of $TiAl_2O_4$%, respectively. The previous interpretation points to the formation of multiple phases in the new material composed of semicrystalline and amorphous phases.

Furthermore, an increase in $TiAl_2O_4$ concentrations increases peak sharpness and hence sample crystallinity, forming a lamellar composite structure. The diffraction peaks that arise are indexing to $TiAl_2O_4$ with a face-centered cubic spinal structure. The $TiAl_2O_4$ spinal phase formed utterly. In addition, there were no impurities found in the prepared sample (Kunde and Sehgal 2020). The Scherer equation estimated the average crystallite size to be around 100 nm.

SEM analysis of prepared membranes

SEM image of blank and PVC-NC@TALCM with different ratios (1, 3, and 5%) in Fig. 6a indicates a stable membrane of PVC-NC@TALCM, which was obtained through the preparation process. We note that the surface of the blank membrane is smooth and flat with the fusion of cellulose nanoparticles with the interior of the prepared membrane. Due to physicochemical interactions, the adsorption layer is internal, not external; a stable matrix forms when NC adds to PVC. The matrix becomes strengthened after adding $TiAl_2O_4$ due to the physical reinforcement. The subsequent addition of $TiAl_2O_4$ to the matrix provides sufficient crosslinking, which enhances the overall functional performance and roughness.

SEM images in Fig. 6b reveal the growth of nano/micro clusters of $TiAl_2O_4$ nanotubes through the membrane surface. The clusters are non-uniform in size and non-regular in shape. The tubes are very slick, with an outer diameter of 550 nm and a tube length of 825 ± 51.7 nm. Figure 6c shows irregular clusters almost similar to the morphology of titanium aluminate nanoparticles in Fig. 6b. Increasing the $TiAl_2O_4$ ratio in the membrane increased the size of overgrowing micro clusters despite a drop in their number. Insets with increased $TiAl_2O_4$, as shown in Fig. 6d, where the $TiAl_2O_4$ appeared as uniform circular holes and in a homogenous distribution.

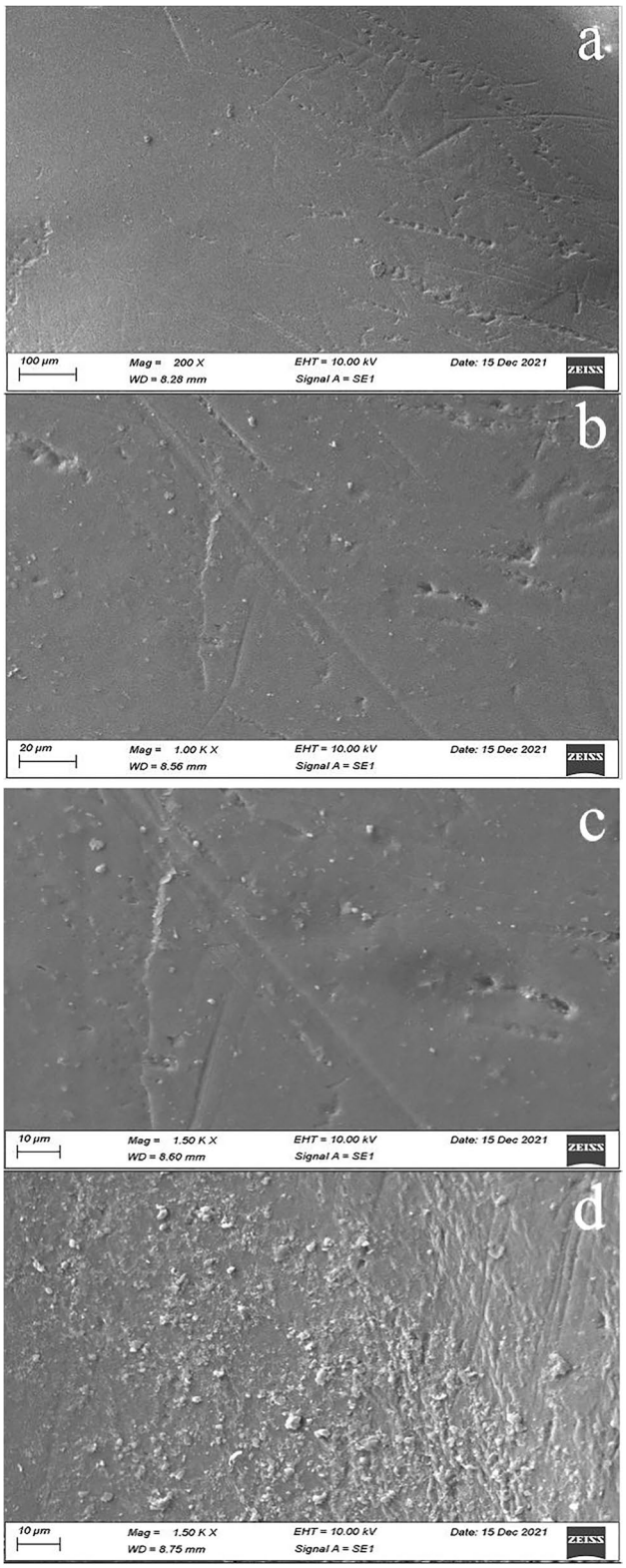

Fig. 6 SEM images of blank (**a**), PVC-NC@TALCM 1% (**b**), PVC-NC@TALCM 3% (**c**), and PVC-NC@TALCM 5% (**d**)

TGA analysis of prepared membranes

By analyzing the thermal stability of the prepared membranes, it can be said that the addition of titanium aluminate ($TiAl_2O_4$) helped in the thermal stability of the primary polymer PVC/NC, as shown in Fig. 7. It is noted that the degradation of PVC/NC occurs in three stages. The first stage is the solvent exit, a tiny stage because a small percentage of the solvent in the membrane ends at 150 °C, followed by a second stage that intersects around the exit of functional groups from the base polymer and ends at 334 °C. The final stage is carbonation, which ends at 485 °C and expresses the gaseous vacuum of carbon gas, affecting the analysis result at the end of the slit.

Like other composites that contain titanium aluminate, the increasing proportion of titanium aluminate in the composite has resulted in an increase in the crushing of materials and an expansion in the extent of the crushing stages. It is noted that the first stage is 150 °C, while the second stage is much at 323, 345, and 246 for the ratios from 1–3% for titanium aluminate, which confirms the high thermal stability of the composite for the original membrane. Also, it is noted that the burnt sample decreased with increased titanium aluminate percentage, confirming its thermal stability. Additionally, the intermediate stages appear for the essential components of the nanomaterials used, Al and TiO_2.

Performance evaluation of adsorption membranes

Effect of initial dye concentrations on the uptake efficiency

The influence of initial dye concentrations on the absorption efficiency of the PVC/NC@TALCM membrane is shown in Fig. 8. With increasing MB concentration, the removal efficiency of PVC/NC@TALCM membrane increased from 65.3 to 83.4%, corresponding to MB concentrations of 10 and 30 ppm in the case of 5% PVC/NC@TAlCM. In contrast, in the case of 3 and 1% membrane ratio, the removal efficiency was 73 and 65.3%, and 41% for PVC/NC, respectively. The adsorption of MB dye on PVC-NC@TALCM membrane is enhanced by increasing the initial concentration of MB dye; this may be due to the complete saturation of the PVC/NC@TAlCM membrane adsorption sites in the case of the 3 and 1% membrane ratio. Whereas, in the case of 5% PVC-NC@TALCM, the increased adsorption of MB dye is most likely due to an increase in the ratio of adsorption sites on the membrane surface compared to the dye concentration, as the driving force generated by increasing the dye concentration increases, and becomes sufficient to overcome the mass transfer between the solid and liquid phases and enhance the adsorption process progress and removal efficiency (Gharbani and Mehrizad 2022).

The adsorption of MB dye on the PVC-NC@TALCM membrane increases with increasing initial concentration due to the availability of more adsorption sites on the membrane surface, resulting in a higher driving force for the adsorption process and an improvement in membrane removal efficiency. However, the relationship between the initial concentration of MB dye and the adsorption capacity of the membrane may not be linear, and there may be a saturation point beyond which further increases in dye concentration do not lead to a corresponding increase in adsorption capacity. Further studies are required to determine the optimal conditions for using this membrane for the effective removal of MB dye from wastewater.

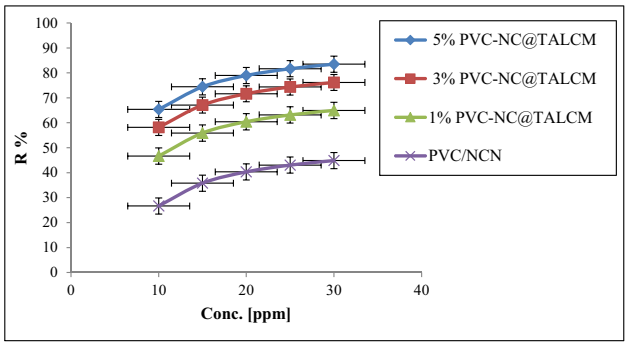

Fig. 8 Effect of initial MB concentrations on the adsorption and removal efficiency

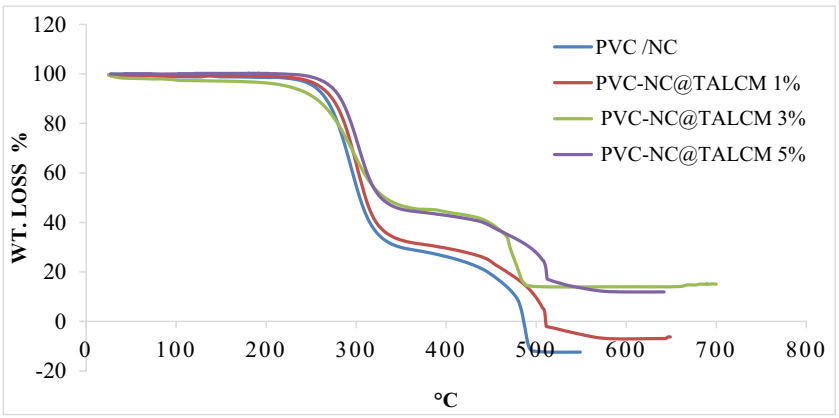

Fig. 7 TGA of PVC-NC and PVC-NC@TALCM with different concentration

Adsorbent dose effect

At all indicated mixing ratios (1, 3, 5%), the maximum removal efficiency of MB dye was (88.2, 97.6, and 98.6%) respectively, as shown in Fig. 9. The presence of different adsorption sites enhanced the available surface area for the adsorption process to complete, leading to a high removal efficiency in the sequence of 5% PVC-NC@TALCM > 3% PVC-NC@TALCM > %1 PVC-NC@TALCM > PVC-NC (Sabarish and Unnikrishnan 2018a, b).

Also, it can say that the $TiAl_2O_4$ composite in the membrane enhances the adsorption process of the dye in cooperation with the cellulose nanoparticle distributed in the polyvinyl chloride supporting membrane layer; this helps to increase the adsorption with an increase in the ratio of the titanium aluminate as shown in Fig. 9.

Effect of pH

The influence of pH on MB adsorption by PVC-NC@TAlCM at different ratios (1, 3, and 5%) membranes was investigated, with the findings shown in Fig. 10. The uptake efficiency initially increased with increasing pH for all composite membrane ratios and reached its maximum at pH = 10; these results agree with many researchers [35]. Increasing the pH of the methylene blue dye solution causes electrostatic reactions between the MB dye and the PVC-NC@TAlCM membrane. It is observed mainly in cases of 5% and 3% with a maximum removal efficiency of 98.6%, leading to an increase in the percentage of negative hydroxyl ion, and this leads to an increase in the dye uptake process on the surface of the nanocomposite membrane (Lu et al. 2018). However, the positive charges on the surface of the PVC-NC@TAlCM adsorbent membrane and the positive charge of the methylene blue dye solution compete at lower pH levels.

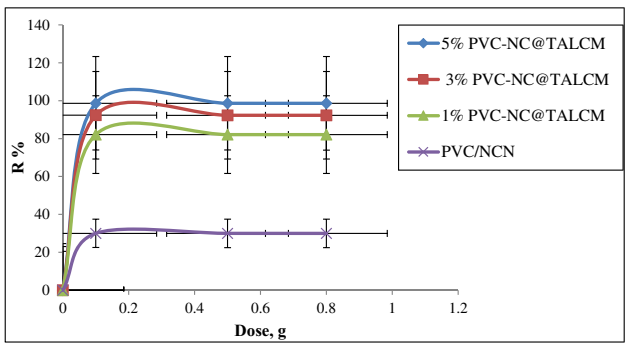

Fig. 9 Effect of adsorbent dose on MB adsorption

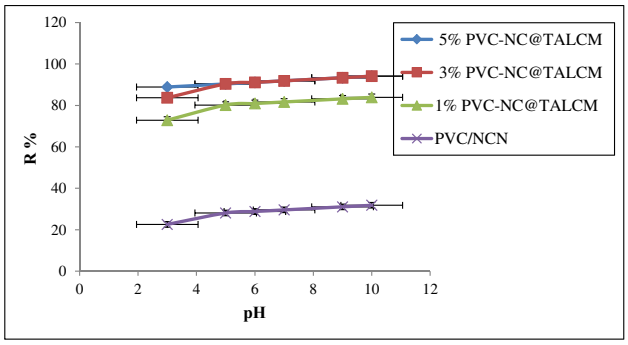

Fig. 10 Effect of pH on the adsorption of MB

Adsorption kinetics

The behavior of uptakes MB by blank and PVC-NC@TALCM nanocomposite adsorption kinetics was investigated using pseudo-first and pseudo-second-order models applied to batch adsorption findings.

The pseudo-first-order model's linear form showing below Eq. 4:

$$\log(q_e - q_t) = \log q_e - \frac{k_1 t}{2.303} \tag{4}$$

where q_e (mg g^{-1}) is the adsorption capacity at equilibrium and q_t (mg g^{-1}) is the adsorption capacity at time t (min), and k_1 (min^{-1}) is the pseudo-first-order rate constant. The slope and intercept of log (q_e-q_t) plots vs. t, as illustrated in Fig. 11, were used to determine the constants q_e, k_1, and correlation coefficients r^2 (Vedula and Yadav 2022).

The linear expression for the pseudo-second-order rate expression is (Eq. 5):

$$\frac{t}{q_t} = \frac{1}{k_2 q_e^2} + \frac{1}{q_e} t \tag{5}$$

Q_e (mg g^{-1}) is the adsorption capacity at equilibrium, and q_t (mg g^{-1}) is the adsorption capacity at time t (min), while k_2 (g mg^{-1} min^{-1}) is the rate constant of pseudo-second-order. It can derive the rate constants k_2, q_e, and correlation coefficients r^2 using linear plots of t/qt vs. t. (Fig. 12).

Two kinetic models' parameters were shown in Table 2, with the correlation coefficient (r^2) in the case of pseudo-first-order kinetic models being 0.79, 0.80, and 0.88 for 1, 3, and 5% of PVC-NC@TALCM, respectively. Whereas, r^2 ranged from 0.99 to 1 in every case when the pseudo-second-order kinetic model was used at 25 °C, indicating that the correlation coefficients (r^2) derived from the pseudo-second-order kinetic model are significantly higher than correlation coefficients derived from the pseudo-first-order kinetic model.

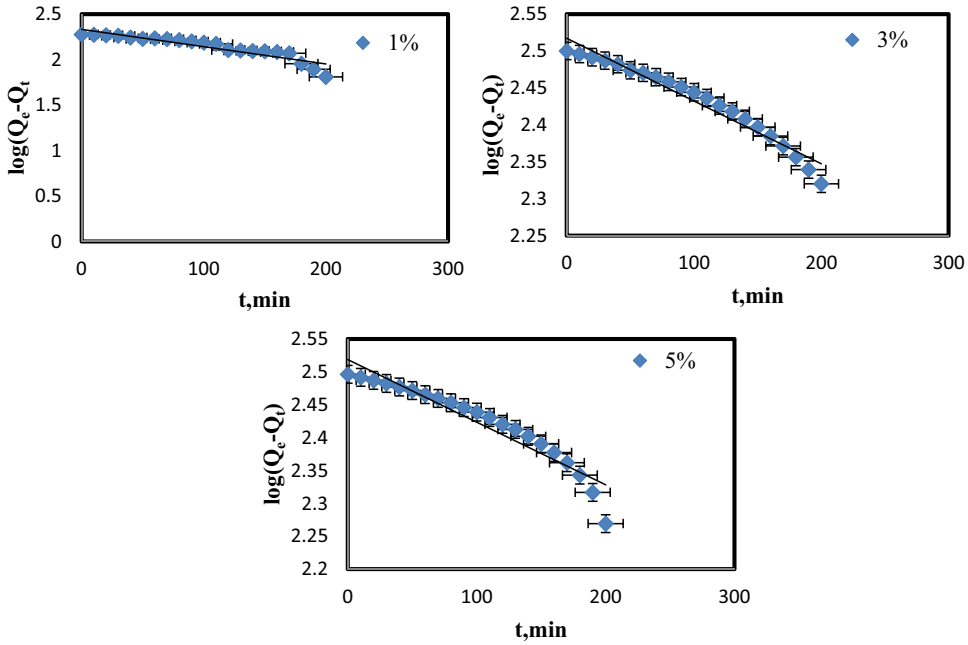

Fig. 11 Pseudo-first-order adsorption of MB on nanocomposite membranes (5, 3, 1%)

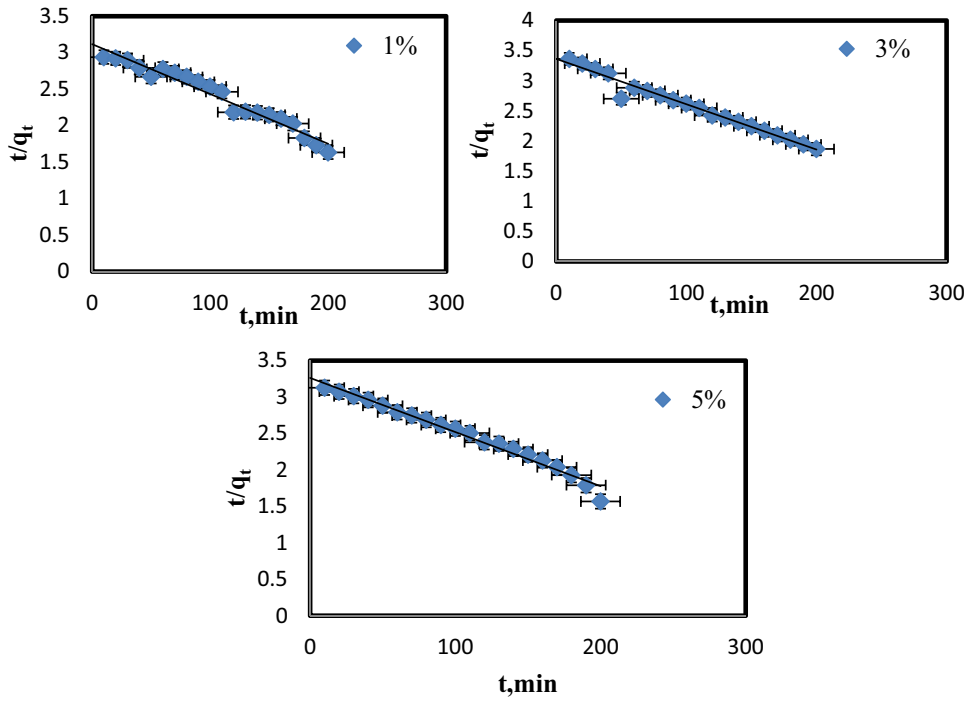

Fig. 12 Pseudo-second-order adsorption of MB on nanocomposite membrane (5, 3, 1%)

We may infer that both variables q_e and r^2 indicated the adsorption of MB onto composite membrane followed the pseudo-second-order kinetic model, indicating that the chemical adsorption process is the rate-limiting step (Hisada et al. 2019).

Adsorption isotherm

The adsorption isotherm was investigated to clarify MB's adsorption performance onto PVC-NC@TALCM membranes. Freundlich and Langmuir's models were applied to discover the appropriate model to explain MB adsorption [39].

Table 2 Calculated kinetic parameters for the adsorption of MB on the membrane

Pseudo-first-order		Pseudo-second-order	
Models	MB	Models	MB
5%			
k_1 (min^{-1})	0.00095	k_2 ($\times 10^{-3}$ g mg^{-1} min^{-1})	1.5243
q_e (Cal) (mg g^{-1})	1.5297	q_e (Cal) (mg g^{-1})	134.69
q_e (Exp) (mg g^{-1})	313.57	q_e, (Exp) (mg g^{-1})	141.83
r^2	0.95	r^2	0.99
3%			
k_1 (min^{-1})	0.000849	k_2 ($\times 10^{-3}$ g mg^{-1} min^{-1})	1.5062
q_e (Cal) (mg g^{-1})	2.2517	q_e, (Cal) (mg g^{-1})	132.801
q_e (Exp) (mg g^{-1})	316.265	q_e (Exp) (mg g^{-1})	140.48
r^2	0.85	r^2	0.98
1%			
k_1 (min^{-1})	0.00160	k_2 ($\times 10^{-3}$ g mg^{-1} min^{-1})	1.2065
q_e (Cal) (mg g^{-1})	4.3533	q_e (Cal) (mg g^{-1})	147.97
q_e (Exp) (mg g^{-1})	367.58	q_e (Exp) (mg g^{-1})	163.28
r^2	0.80	r^2	0.98

C_e is the equilibrium concentration of adsorbate (mg/l) in the Freundlich and Langmuir model, and q_e (mg/g) is the adsorbent's equilibrium adsorption capacity. In contrast, q_m (mg/g) is the maximum adsorption capacity. Table 3 illustrates the linear form of this model.

Freundlich and Langmuir constants (L/mg) are denoted by K_L and K_f, respectively. n denotes the adsorption intensity, while K_f denotes the maximal adsorption capacity (mg/g). The slope and intercept of the plot C_e/q_e vs. C_e were used to get the Langmuir maximum uptake q_m and K_L; the Freundlich constants n and K_f were determined by plotting ln q_e versus ln C_e.

Adsorption favorability was typically predicted using the value of $1/n$. If $1/n = 0$, adsorption is irreversible, beneficial if $(0 < 1/n < 1)$, and unfavorable if $1/n > 1$ (Hebbar et al. 2018).

Table 3 displays the isotherm constants determined by linearly fitting the experimental data, (Figs. 13, 14). The current experimental findings fit the Freundlich model of adsorption in all cases. This result shows that incorporating $TiAl_2O_4$ into PVC-NC@TALCM alters the membrane surface and enhances an adsorption protocol described by Freundlich.

The Langmuir and Freundlich isotherms were used to characterize the connection between the number of MB adsorbed and its equilibrium concentration in solution at room temperature, the findings are shown in Table 3.

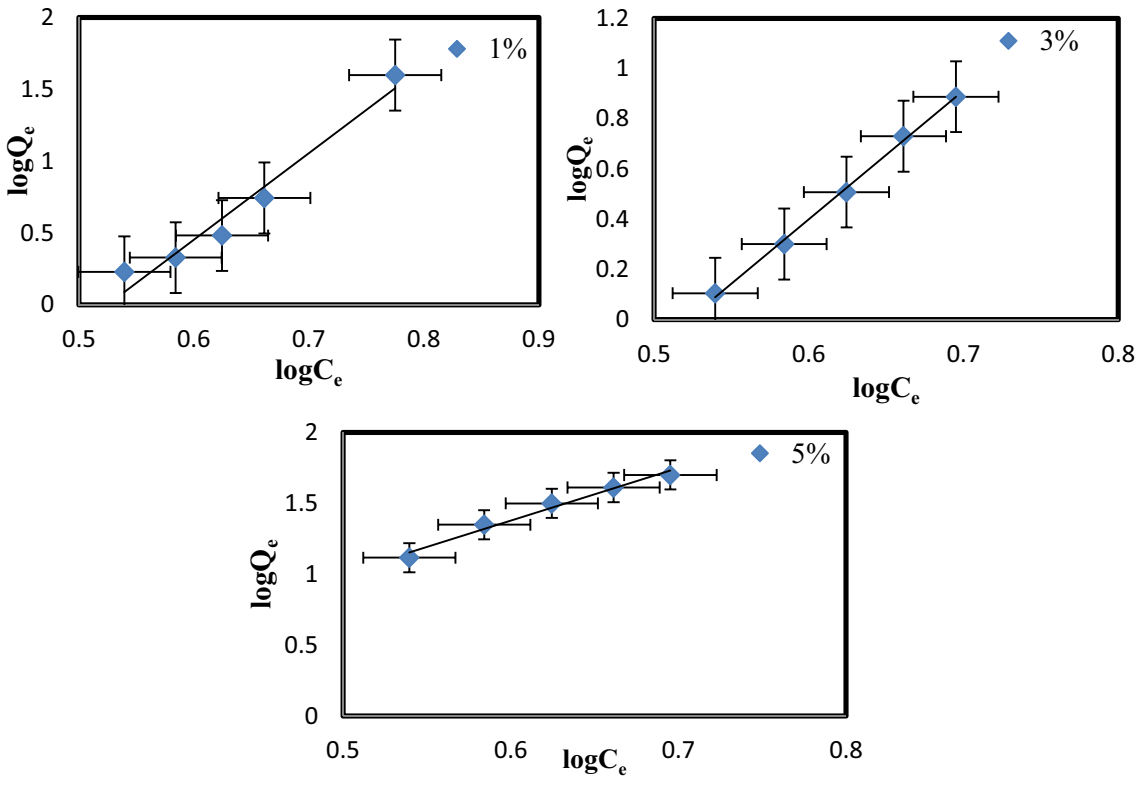

Fig. 13 Freundlich adsorption isotherm of MB onto PVC-NC@TAlCM (1, 3, 5%) nanocomposite

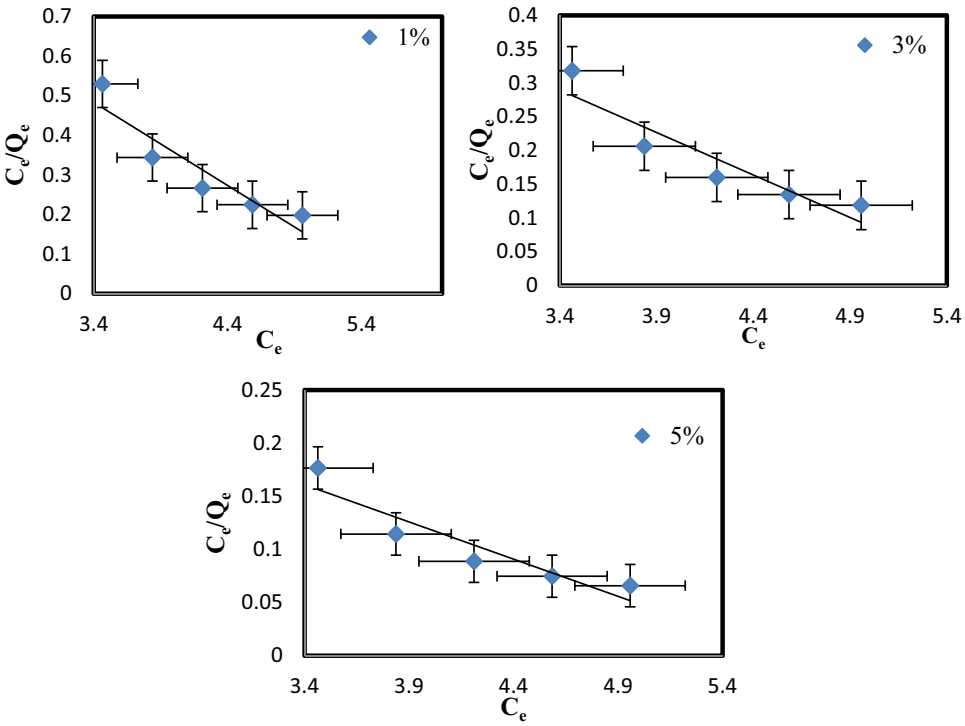

Fig. 14 Langmuir adsorption isotherm of MB onto PVC-NC@TAlCM (1, 3, 5%) nanocomposite

Adsorption thermodynamic

Thermodynamics studies also elucidate adsorption mechanisms. *K*c, Δ*S*, Δ*G*, and Δ*H* for adsorption were calculated by Vant Hoffer equation (Eq. 6, 7 and 8), as shown in Fig. 15.

$$k_c = \frac{q_e}{c_e} \tag{6}$$

$$\ln k_c = \left(\frac{\Delta S}{R}\right) - \left(\frac{\Delta H}{R \times T}\right) \tag{7}$$

Table 3 Langmuir's and Freundlich calculated isotherms

Isotherm equation	Langmuir	Isotherm constant	Freundlich
5%			
q_m (mg/g)	14.2974	K_f	2.3302
K_L(L/mg)	35.8582	n	0.26
r^2	0.92	r^2	0.99
3%			
q_m (mg/g)	7.94305	K_f	14.55
K_L(L/mg)	11.06735	n	0.19
r^2	0.93	r^2	0.99
1%			
q_m (mg/g)	4.7654	K_f	23.5695
K_L(L/mg)	3.9842	n	0.16
r^2	0.92	r^2	0.985

$$\Delta G = -R \times T \times \ln K_c \tag{8}$$

T (K) is the absolute temperature, and R (8.314 Jmol^{-1} K^{-1}) is the universal gas constant. At the same time, K_c is the thermodynamic equilibrium constant at different temperatures, Δ*G* is the Gibbs' free energy in kJ mol^{-1}, Δ*H* is the enthalpy change in kJ mol^{-1}, and Δ*S* is the entropy change in J mol^{-1} K^{-1} (Gharbani and Mehrizad 2022).

The calculated values for all parameters at MB C0=200 mg L^{-1} were indicated in Table 4. For the adsorption system, Δ*G* was negative for all ratios. As a result, physical adsorption occurred spontaneously. The negative Δ*G* value of MB adsorption by membrane surface increased as the temperature rose in all cases, indicating that the MB dye's adsorption strength also increased. Because of the positive Δ*H* (24,705.2, 26,974.01, 29,391.36 Jmol^{-1}) for 1, 3, and 5% of PVC-NC@TAlCM, respectively, MB adsorption is endothermic. The positive Δ*S* (55.19024, 61.45884, 67, 99863 J mol^{-1} K^{-1}) for 1, 3, and 5% PVC-NC@TAlCM, respectively, indicated that the membrane surface had high MB affinity (Gohr et al. 2022).

Self-cleaning properties of prepared membrane based on contact angle measurement

It is essential to know that the contact angle measurement only indicates the self-cleaning behavior of the membrane surface. Based on the contact angle measurements, the PVC/nanocellulose@$TiAl_2O_4$ membrane exhibits a low contact angle, indicating that the surface is hydrophilic and may

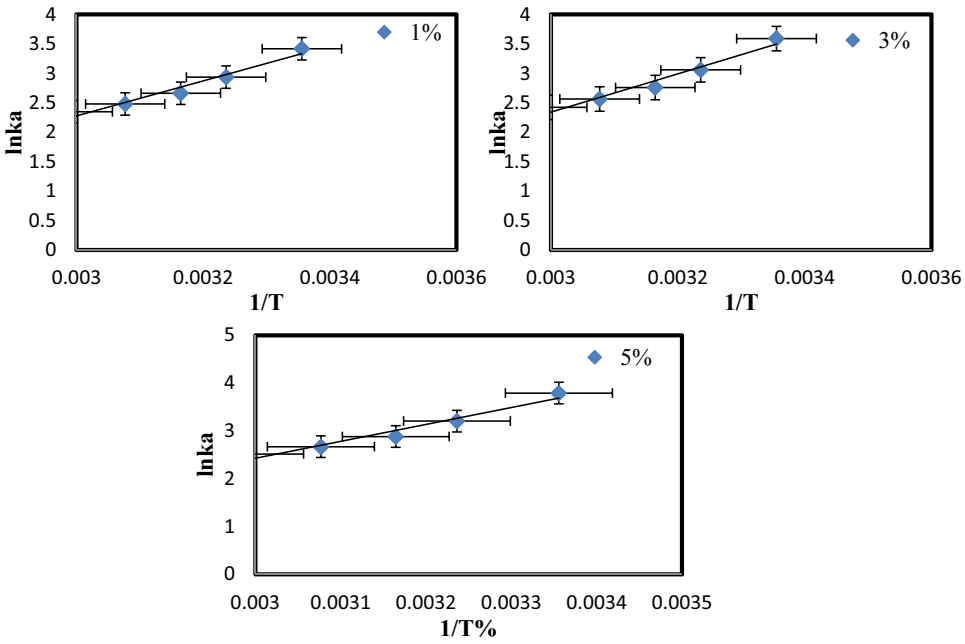

Fig. 15 The linear form of vant Hoff equation of PVC-NC@TAlCM (1, 3, 5%) nanocomposite

Table 4 Thermodynamic parameters of the adsorption process at different temperatures

T (°C) MB	Δ*G* (J/mol)	Δ*S* (J/mol K)	Δ*H* (J/mol)
5%			
25	− 9389.04	67.99863	29,391.36
36	− 8233.35		
43	− 7568.07		
52	− 7208.97		
61	− 6985.23		
3%			
25	− 8892.87	61.45884	26,974.01
36	− 7854.77		
43	− 7249.98		
52	− 6924.31		
61	− 6721.75		
1%			
25	− 8462.78	55.19024	24,705.18
36	− 7543.49		
43	− 6994.95		
52	− 6699.45		
61	− 6515.63		

exhibit self-cleaning behavior. Our measurements yielded an average contact angle of 43°, which is lower than the control sample (PVC/NC) which recorded 89.5°, and by comparing our results with the previous studies on hydrophilic membranes, it is found that the measured contact angles of casting PVC/nanocellulose@$TiAl_2O_4$ membrane films are in line with recent literature values (Hurwitz et al. 2010). It can be said that the PVC/nanocellulose@$TiAl_2O_4$ membrane exhibits a self-cleaning property based on the low contact angle (43°) measurement. This property is likely due to the combined effect of the $TiAl_2O_4$ nanoparticles and the nano cellulose fibers on the surface of the membrane.

Additionally, the results can suggest that the PVC/nanocellulose@$TiAl_2O_4$ membrane surface has high surface energy, which can prevent the adhesion and accumulation of MB dye. This is due to the hydrophilicity of the $TiAl_2O_4$ nanoparticles and the high roughness of combined nano cellulose fibers, which create a hierarchical roughness on the surface of the membrane. This roughness can trap air pockets, preventing contact with the water droplets and promoting the self-cleaning effect in the case of MB dye filtration (Hui Ting et al. 2023).

Adsorption process mechanism

The possible adsorption mechanism of MB on the surface of (PVC/NC@TAlCM) was illustrated in Fig. 16. According to the existing functional groups on the (PVC/NC@TAlCM) surface, the MB adsorption mechanism can be assigned to the various interactions such as electrostatic, hydrogen bonding interactions, van der Waals, and π-π stacking. Therefore, the zeta potential was examined to understand better the contact forces between the membrane surface and the MB. The zeta potential of the modified membrane surface was 4.8–1.2 mV at pH 3 and 10, suggesting that the electrostatic interaction was the most important contact between the composite membrane surface and the MB. That means, the adsorption of MB from aqueous solution by (PVC/NC@TAlCM) is strongly dependent on the interaction of the polar functional groups

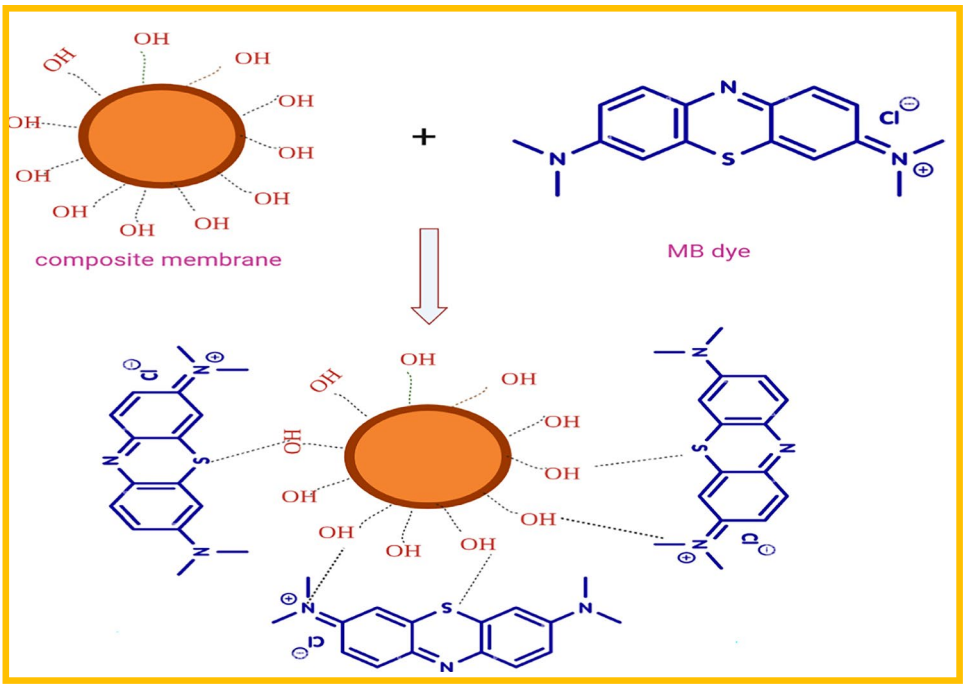

Fig. 16 Zeta potential curve as a function of solution pH obtained for (PVC/NC@ TAlCM)

($-SO_3$) of MB molecule with the OH group of the composite membrane surface (PVC/NC@TAlCM). Similar observations have been reported for the adsorption of MB on other surfaces (Wang et al. 2022a, b, c).

The novelty of the prepared nanocomposite (PVC-NC@$TiAl_2O_4$)

To increase the water treatment operating efficiency process and energy savings, the nanofiltration membranes were prepared for semi-industrial purposes. Therefore, a new nanofiltration membranes (PVC/NC) with excellent initial separation performance for industrial wastewater treatment were synthesized and integrated with nano-sized $TiAL_2O_4$ to be more flexible, durable, and high biological and chemical resistance. Additionally, the self-cleaning is also possible, enhancing chemical properties and reducing the number of chemicals used.

For this purpose, polyvinyl chloride-nanocellulose (PVC/NC) membranes are prepared by the phase inversion method (by dissolving and blending PVC and NC solution). In addition, varying amounts of nano-sized $TiAl_2O_4$ are employed as an adsorbent to generate nanocomposite membranes with high removal efficiency. The impact of the polymer binder blend ratio (PVC to NC) and $TiAl_2O_4$ concentration on the physicochemical properties of membranes is also investigated.

Based on Table 5, it appears that the nanofiltration membranes (PVC-NC@ $TiAl_2O_4$) have a high rejection rate of 98.6% for MB dyes with an initial concentration of 150 mg/L. This is a significant result, as it indicates that the nanofiltration membranes are effective at removing the dyes from the solution.

As illustrated in Table 5, when comparing the result of PVC-NC@ $TiAl_2O_4$ membranes with other adsorbents and membrane types, it appears that the PVC-NC@ $TiAl_2O_4$ membranes are among the most effective at removing dyes. In fact, their rejection rate is higher than that of most of the other adsorbents and membranes listed.

It is important to note that the effectiveness of a particular adsorbent or membrane will depend on the specific pollutant being targeted, as well as other factors such as the initial concentration of the pollutant and the conditions under which the adsorption or filtration is taking place. However, based on the information in Table 5, it appears that the PVC-NC@ $TiAl_2O_4$ membranes are a promising choice for dye removal. Overall, the high rejection rate of the PVC-NC@ $TiAl_2O_4$ membranes suggests that they are a promising technology for dye removal. However, further research is needed to determine their effectiveness under different conditions and for different types of dyes.

Conclusion

Novel PVC-NC@TALCM nanocomposite filtration membranes were successfully prepared by adding $TiAl_2O_4$, effectively modifying the PVC-NC@TALCM matrix according to XRD, FTIR, SEM, and TGA for the removal of methyl blue from industrial wastewater. The efficiency of 5, 3, and

Table 5 Various adsorption-membrane systems for various pollutants removal

Type of membranes	Type of adsorbents	C_0, mg/l	*R*%	Pollutants	Ref
UF	(PVA/PDADMAC/ZSM-5)	20	95%	Methyl orange dye	(Sabarish and Unnikrishnan 2018a, b)
NF	CuTz-1/graphene oxide (CuTz-1/GO)	50	94.9%	Methylene blue dye	(Zhou et al. 2021)
MF	Powdered activated carbon	50	90%	Synthetic organic contaminants	(Li 2014)
UF	(PVA/CMC/ZSM-5 zeolite)	100	97%	Methylene blue dye	(Sabarish and Unnikrishnan 2018a, b)
UF	Bentonite	50	97%	Methylene blue dye	(Al-Bastaki and Banat 2004)
NF	(PVC-NC@TALCM)	150	98.6%	Present study	

1% PVC/NC@TALCM nanocomposite membrane was 98.6, 92.29, and 82.09%, respectively, at pH 10 and 30 ppm (initial dye concentration). The Freundlich model can describe the adsorption isotherm of MB on PVC-NC@TALCM nanocomposite membrane, and the adsorption kinetics followed the pseudo-second-order model for all ratios. Maximum adsorption capacity (q_e) was found to be 134.69 mg g^{-1}. The adsorption process was found to be spontaneous and endothermic, accompanied by an increase in entropy. It was concluded that the PVC-NC@TALCM nanocomposite membrane was an economical, environmentally friendly adsorbent for removing MB from industrial wastewater. In addition, it is self-cleaning, which helps in sustainability and will enhance the chemical properties and capabilities of the nanocomposite membranes by reducing the number of chemicals.

Acknowledgements BioRender carried out Figures 1, 2, 3, 6, and 16. This paper is based upon work supported by Science Technology & Innovation Funding Authority (STDF) under a grant (call1/Post Graduate Support Grant (PGSG) (ID 44668).

Author contribution Original idea: MFM, MK, IEE, and TA. Experiment design: AAE and MFM. Measurement: AAE, MFM, and M.K. Data analysis: AAE, MFM, and MK. Manuscript preparation and revisions: AAE, MFM, MK, IEE, and TA.

Funding Open access funding provided by The Science, Technology & Innovation Funding Authority (STDF) in cooperation with The Egyptian Knowledge Bank (EKB). This paper is based upon work supported by Science Technology & Innovation Funding Authority (STDF) under a grant (call1/Post Graduate Support Grant (PGSG) (ID 44668).

Data availability The datasets used and analyzed during the current study are available from the corresponding author upon reasonable request.

Code availability Not applicable.

Declarations

Ethics approval and consent to participate Not applicable.

Consent for publication Not applicable.

Conflict of interest The authors declare no competing interests.

References

Agarwalla A, Mohanty K (2022) Comprehensive characterization, development, and application of natural/Assam Kaolin-based ceramic microfiltration membrane. Mater Today Chem 23:100649

Ahmad T, Guria C (2022) Progress in the modification of polyvinyl chloride (PVC) membranes: a performance review for wastewater treatment. J Water Process Eng 45:102466

Al-Bastaki N, Banat F (2004) Combining ultrafiltration and adsorption on bentonite in a one-step process for the treatment of colored waters. Resour Conserv Recycl 41(2):103–113

Chen R, Ma Z, Sun D, Wang X, Han Y (2022) Cellulose I nanocrystals (CNCs I) prepared in mildly acidic lithium bromide trihydrate (MALBTH) and their application for stabilizing Pickering emulsions. Int J Biol Macromol 201:59–66

Debnath B, Haldar D, Purkait MK (2021) A critical review on the techniques used for the synthesis and applications of crystalline cellulose derived from agricultural wastes and forest residues. Carbohyd Polym 273:118537

Deng W, Li Y (2021) Novel superhydrophilic antifouling PVDF-BiOCl nanocomposite membranes fabricated via a modified blending-phase inversion method. Sep Purif Technol 254:117656

Fahoul Y, Zouheir M, Tanji K, Kherbeche A (2021) Synthesis of a novel ZnAl2O4/CuS nanocomposite and its characterization for photocatalytic degradation of acid red 1 under UV illumination. J Alloy Compd 889:161708

Gharbani P, Mehrizad A (2022) Preparation and characterization of graphitic carbon nitrides/polyvinylidene fluoride adsorptive membrane modified with chitosan for Rhodamine B dye removal from water: adsorption isotherms, kinetics and thermodynamics. Carbohyd Polym 277:118860

Gidstedt S, Betsholtz A, Falås P, Cimbritz M, Davidsson Å, Micolucci F, Svahn O (2022) A comparison of adsorption of organic micropollutants onto activated carbon following chemically enhanced primary

treatment with microsieving, direct membrane filtration and tertiary treatment of municipal wastewater. Sci Total Environ 811:152225
Hebbar RS, Isloor AM, Abdullah MS, Ismail AF, Asiri AM (2018) Fabrication of polyetherimide nanocomposite membrane with amine functionalised halloysite nanotubes for effective removal of cationic dye effluents. J Taiwan Inst Chem Eng 93:42–53
Hisada M, Tomizawa Y, Kawase Y (2019) Removal kinetics of cationic azo-dye from aqueous solution by poly-γ-glutamic acid biosorbent: contributions of adsorption and complexation/precipitation to Basic Orange 2 removal. J Environ Chem Eng 7(3):103157
Hui Ting LL, Teow YH, Mahmoudi E, Ooi BS (2023) Development and optimization of low surface free energy of rGO-PVDF mixed matrix membrane for membrane distillation. Sep Purif Technol 305:122428
Hurwitz G, Guillen GR, Hoek EMV (2010) Probing polyamide membrane surface charge, zeta potential, wettability, and hydrophilicity with contact angle measurements. J Membr Sci 349(1):349–357
Ismail MF, Islam MA, Khorshidi B, Tehrani-Bagha A, Sadrzadeh M (2022) Surface characterization of thin-film composite membranes using contact angle technique: review of quantification strategies and applications. Adv Coll Interface Sci 299:102524
Jain H, Kumar A, Rajput VD, Minkina T, Verma AK, Wadhwa S, Dhupper R, Chandra Garg M, Joshi H (2022) Fabrication and characterization of high-performance forward-osmosis membrane by introducing manganese oxide incited graphene quantum dots. J Environ Manage 305:114335
Kunde GB, Sehgal B (2020) Eco-designed iron aluminate (FeAl2O4) free-standing mesoporous films and supported ultrafiltration membranes for wastewater treatment. J Environ Chem Eng 8(5):104201
Li M (2014) Effects of natural organic matter on contaminant removal by superfine powdered activated carbon coupled with microfiltration membranes
Lu Y, Fang Y, Xiao X, Qi S, Huan C, Zhan Y, Cheng H, Xu G (2018) Petal-like molybdenum disulfide loaded nanofibers membrane with superhydrophilic property for dye adsorption. Colloids Surf, A 553:210–217
Nthunya LN, Bopape MF, Mahlangu OT, Mamba BB, Van der Bruggen B, Quist-Jensen CA, Richards H (2022) Fouling, performance and cost analysis of membrane-based water desalination technologies: a critical review. J Environ Manage 301:113922
Oladoye PO, Ajiboye TO, Omotola EO, Oyewola OJ (2022) Methylene blue dye: toxicity and potential elimination technology from wastewater. Results Eng 16:100678
Pan Z, Xin H, Xu S, Xu R, Wang P, Yuan Y, Fan X, Song Y, Song C, Wang T (2022) Preparation and performance of polyaniline modified coal-based carbon membrane for electrochemical filtration treatment of organic wastewater. Sep Purif Technol 287:120600
Pankiew A, Chaisriratanakul W, Bunjongpru W, Srisuwan A, Jeamsaksiri W, Thornyanadacha N, Pengpad P, Chauyrod K, Horprathum M (2021) Modification of polyvinyl chloride membranes for mycotoxins detection. Sens Bio-Sens Res 34:100460
Park K, Jang YH, Chang JW, Yang DR (2021) Membrane transport behavior characterization method with constant water flux in pressure-assisted forward osmosis. Desalination 498:114738
Perumal AB, Nambiar RB, Sellamuthu PS, Sadiku ER, Li X, He Y (2022) Extraction of cellulose nanocrystals from areca waste and its application in eco-friendly biocomposite film. Chemosphere 287:132084
Rana AK, Gupta VK, Saini AK, Voicu SI, Abdellattifaand MH, Thakur VK (2021) Water desalination using nanocelluloses/cellulose derivatives based membranes for sustainable future. Desalination 520:115359
Sabarish R, Unnikrishnan G (2018) Polyvinyl alcohol/carboxymethyl cellulose/ZSM-5 zeolite biocomposite membranes for dye adsorption applications. Carbohyd Polym 199:129–140
Sabarish R, Unnikrishnan G (2018b) PVA/PDADMAC/ZSM-5 zeolite hybrid matrix membranes for dye adsorption: fabrication, characterization, adsorption, kinetics and antimicrobial properties. J Environ Chem Eng 6(4):3860–3873
Gohr M, Abd-Elhamid AI, El-Shanshory AA, Soliman HMA (2022) Adsorption of cationic dyes onto chemically modified activated carbon: kinetics and thermodynamic study. J Mol Liq 346:118227
Shaheen TI, Emam HE (2018) Sono-chemical synthesis of cellulose nanocrystals from wood sawdust using acid hydrolysis. Int J Biol Macromol 107:1599–1606
Sun F, Yang J, Shen Q, Li M, Du H, Xing DY (2021) Conductive polyethersulfone membrane facilely prepared by simultaneous phase inversion method for enhanced anti-fouling and separation under low driven-pressure. J Environ Manage 297:113363
Sunil K, Sherugar P, Rao S, Lavanya C, Balakrishna GR, Arthanareeswaran G, Padaki M (2021) Prolific approach for the removal of dyes by an effective interaction with polymer matrix using ultrafiltration membrane. J Environ Chem Eng 9(6):106328
Teng D, Xu Y, Zhao T, Zhang X, Li Y, Zeng Y (2022) Zein adsorbents with micro/nanofibrous membrane structure for removal of oils, organic dyes, and heavy metal ions in aqueous solution. J Hazard Mater 425:128004
TesfayeJule L, Ramaswamy K, Bekele B, Saka A, Nagaprasad N (2021) Experimental investigation on the impacts of annealing temperatures on titanium dioxide nanoparticles structure, size and optical properties synthesized through sol-gel methods. Mater Today: Proceed 45:5752–5758
Ha NTT, Van Giap T, Trong Thanh N (2020) Synthesis of lithium aluminate for application in radiation dosimetry. Mater Lett 267:127506
Vedula SS, Yadav GD (2022) Wastewater treatment containing methylene blue dye as pollutant using adsorption by chitosan lignin membrane: development of membrane, characterization and kinetics of adsorption. J Indian Chem Soc 99(1):100263
Vincent S, Kandasubramanian B (2021) Cellulose nanocrystals from agricultural resources: Extraction and functionalisation. Eur Polymer J 160:110789
Voisin H, Falourd X, Rivard C, Capron I (2021) Versatile nanocellulose-anatase TiO2 hybrid nanoparticles in Pickering emulsions for the photocatalytic degradation of organic and aqueous dyes. JCIS Open 3:100014
Wang K, Yu S, Yin X, Liu L, Wang L, Zhu G, Wang J, Li Q, Yang X (2022) Preparation of ZnS superhydrophobic coating on 316L stainless steel with self-cleaning property and excellent stability. Colloids Surf, A 633:127871
Wang Q, Wang Z, Ding K, Wang L, Gao C, Zhu G (2021) Novel amidoxime-functionalized SBA-15-incorporated polymer membrane-type adsorbent for uranium extraction from wastewater. J Water Process Eng 43:102316
Wang X, Dong J, Gong C, Zhang S, Yang J, Zhang A, Feng Z (2022) Bendable poly(vinylidene fluoride)/polydopamine/β-cyclodextrin composite electrospun membranes for highly efficient and bidirectional adsorption of cation and anion dyes from aqueous media. Compos Sci Technol 219:109256
Wang Y, Jiao Z, Li W, Zeng S, Deng J, Wang M, Ren L (2022c) Superhydrophilic membrane with photo-Fenton self-cleaning property for effective microalgae anti-fouling. Chin Chem Lett: 108020.
Zhou S, Feng X, Zhu J, Song Q, Yang G, Zhang Y, Van der Bruggen B (2021) Self-cleaning loose nanofiltration membranes enabled by photocatalytic Cu-triazolate MOFs for dye/salt separation. J Membr Sci 623:119058